AD-A193 623 HIGH POWER STORAGE SYSTEM BASED ON THIN FILM SOLID IONICS(U) PARIS-6 UNIV (FRANCE) LABORATOIRE DE PHYSIQUE DES SOLIDES M BALKANSKI ET AL. FEB 88 R/D-4867-PH-01 1/1

UNCLASSIFIED DAJA45-85-C-0020 F/G 20/12 NL

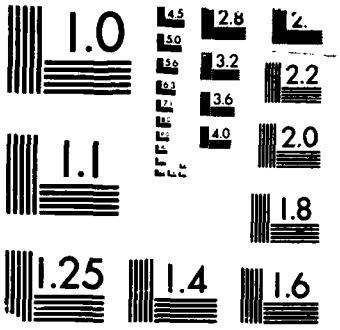

HIGH POWER STORAGE SYSTEM BASED ON THIN FILM SOLID IONICS

M. BALKANSKI and C. JULIEN

Laboratoire de Physique des Solides
de l'Université Pierre & Marie Curie

Contract Number DAJA 45-85-C-0020

Final Report

July 1985 - February 1988

The Research reported in this document has been made possible through the support and sponsorship of the U.S. Government through its European Research Office of the U.S. Army. ~~This report is intended only for the internal menagment use of the Contracter of the U.S. Government.~~

Unclassified
SECURITY CLASSIFICATION OF THIS PAGE

REPORT DOCUMENTATION PAGE

Form Approved
OMB No 0704-0188
Exp Date Jun 30, 1986

1a REPORT SECURITY CLASSIFICATION Unclassified	1b. RESTRICTIVE MARKINGS
2a SECURITY CLASSIFICATION AUTHORITY	3. DISTRIBUTION / AVAILABILITY OF REPORT Approved for public release; distribution unlimited
2b. DECLASSIFICATION / DOWNGRADING SCHEDULE	
4. PERFORMING ORGANIZATION REPORT NUMBER(S)	5. MONITORING ORGANIZATION REPORT NUMBER(S) R&D 4867-PH-01
6a. NAME OF PERFORMING ORGANIZATION Universite Pierre et Marie Curie 6b. OFFICE SYMBOL (If applicable)	7a. NAME OF MONITORING ORGANIZATION USARDSG-UK
6c. ADDRESS (City, State, and ZIP Code) Laboratoire de Physique des Solides, 4 Place Jussieu, Tour 13.2 etage, 75252 Paris Cedex, France	7b. ADDRESS (City, State, and ZIP Code) Box 65 FPO NY 09510-1500
8a. NAME OF FUNDING / SPONSORING ORGANIZATION USARDSG-UK ARO-E 8b OFFICE SYMBOL (If applicable)	9 PROCUREMENT INSTRUMENT IDENTIFICATION NUMBER DAJA45-85-C-0020
8c. ADDRESS (City, State, and ZIP Code) Box 65 FPO NY 09510-1500	10. SOURCE OF FUNDING NUMBERS

PROGRAM ELEMENT NO	PROJECT NO	TASK NO	WORK UNIT ACCESSION NO
61102A	1L161102BH57	07	

11 TITLE (Include Security Classification)

(U) High Power Storage System Based on Thin Film Solid Ionics

12 PERSONAL AUTHOR(S)
Professor M. Balkanski

13a TYPE OF REPORT	13b TIME COVERED FROM _____ TO _____	14 DATE OF REPORT (Year, Month, Day)	15 PAGE COUNT

16 SUPPLEMENTARY NOTATION

17 COSATI CODES			18. SUBJECT TERMS (Continue on reverse if necessary and identify by block number)
FIELD	GROUP	SUB-GROUP	
20	12		
10	02		

19 ABSTRACT (Continue on reverse if necessary and identify by block number)

20 DISTRIBUTION / AVAILABILITY OF ABSTRACT	21 ABSTRACT SECURITY CLASSIFICATION
☒ UNCLASSIFIED/UNLIMITED ☒ SAME AS RPT ☒ DTIC USERS	Unclassified

22a NAME OF RESPONSIBLE INDIVIDUAL	22b TELEPHONE (Include Area Code)	22c OFFICE SYMBOL
Dr. Gerald R. Andersen	01-409 4423	AMXSN-UK-RP

DD FORM 1473, 84 MAR 83 APR edition may be used until exhausted
All other editions are obsolete

SECURITY CLASSIFICATION OF THIS PAGE
Unclassified

Summary

Thin film insertion cathode have been obtained in the In-Se system and Hall mobility up to 50 $cm^2V^{-1}s^{-1}$ have been measured on annealed films. Electrochemical lithium intercalation has been performed and shows that a plateau appears at 1.8V. The redox stability range has been determined by cyclic voltametry for different preparation conditions of the films.

Lithium solid state hybrid systems using borate glasses as electrolyte and lamellar compounds as intercalated electrode have been tested from the point of view of storage applications. The secondary prototype built with a composite electrode including $NiPS_3$, carbon and powdered electrolyte have been set up and checked. Both thermodynamic and kinetic parameters are given under high power storage conditions.

A. INTRODUCTION

This report deals with the laboratory scale studies of solid state batteries working at room temperature according to the scheme

Alkali	//	Fast ion conducting glass	//	Insertion
Metal	//	$B_2O_3 + Li_2O$ + salt	//	Compound

It is well known now that fast ion conducting glass electrolytes are enough good ionic conductors for secondary batteries and have the advantages to present a large stability range when alkali metal is used as electrode ion-reservoir, a very low electronic conductivity at room temperature (Menetrier et al., 1984) and are easily formed into complex shapes when accommodate with other components in the system.

All solid microbatteries are currently being investigated for use in micro electronic devices (Kanehori et al., 1983) and recent studies have shown that the use of indium selenide as the insertion cathode material is possible (Julien and Hatzikraniotis, 1987). During the discharge process, this material serves as an ionic conductor for the cation Li^+ ; this property along with the high values of electrical conductivity, lithium diffusity and electrochemical potential relative to lithium, make InSe a quite favourable material for battery operation in thin film technology.

Material	Unit cell (nm)	Conductivity (S/cm)	Energy gap (eV)
InSe	a = 0.4002 b = 0.831	0.01 - 0.2	E^d_g = 1.29 E^i_g = 1.19
GaSe	a = 0.3755 b = 0.797	5 - 15	E^d_g = 2.13 E^i_g = 2.1
MoS_2	a = 0.316 b = 0.615	0.03	E^d_g = 1.74 E^i_g = 1.10
In_2Se_3	a = 0.402 b = 1.934	1 - 10	E^d_g = 1.24 E^i_g = 1.10
TiS_2	a = 0.341 b = 0.569	10 - 100	E^d_g = 0.2

Table 1 : Characteristics of different layered materials which can be used as insertion cathodes in solid state batteries.

Results on hybrid solid state batteries, are also presented here. There are minigenerators with thickness higher than that of thin film batteries and can store larger specific capacity using different insertion cathodes, whose list is given in table 1.

B. THIN FILM SOLID STATE BATTERIES

1. Thin film insertion cathode

In the progress reports, we have discussed the structural properties of In_xSe_{1-x} thin films. It has been established that the flash evaporation technique leads to good In-Se stoichiometry with acceptable reproducibility. This is an important factor for lithium micro-battery in which the electronic conductivity of the insertion cathode plays an important role in the battery operation.

Electrical resistivity and Hall measurements are performed using the five-probe technique. Ohmic contacts are provided by evaporation of In spots on the films. The polycrystalline films are formed by subsequent thermal annealings with T_a ranging from 300 K to 600 K, in a purified flowing argon atmosphere. All flash evaporation films are initially n-type semiconductor.

Figure 1 represents the variation of the Hall mobility of thin film prepared at T_s=433 K as a function of the isothermal annealing time.

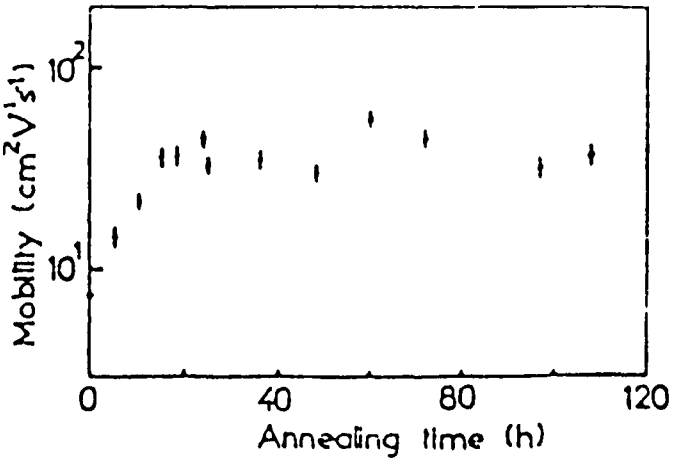

Fig.1 Hall mobility versus annealing time for InSe thin films prepared at T_s=433K.

The optimum value appears after few hours ; after 15 hours under inert atmosphere of annealing, the Hall mobility remains stable and constant at 50 cm^2/Vs, while the carrier concentration does not change notably. The Hall mobility increases consequently with the annealing temperature T_a, but temperature of about 600 K seems to be an upper limit, because higher annealing temperature induces chemical reactions (figure 2). The apparent decomposition can be attributed to the evaporation of Se atoms. The film's Hall mobility remains weak compared to the crystal's, which can reach 10^3 cm^2/Vs at RT.

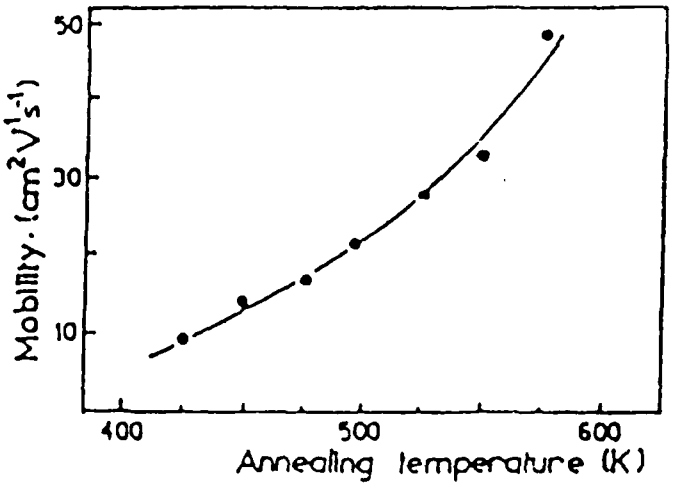

Fig.2 Hall mobility versus annealing temperature for InSe thin films prepared at T_S=433 K.

The electrical conductivity shows an exponential behaviour as a function of temperature and the activation energy decreases as annealing temperature increases. The room temperature conductivity increases by three orders of magnitude when the annealing temperature rises from 300 K up to 575 K ; for T_a > 575 K the electrical conductivity remains constant (Guesdon et al., 1987).

The electrical transport properties of InSe films are governed by carrier trapping at the grain boundaries (Petritz, 1956). To simplify the model, we assume that the films are composed of identical crystallites having a grain size L, and that only one type of totally ionized impurity is present. The energy band diagram in the crystallites, is calculated using an abrupt depletion approximation. For a higher potential barrier height the values of the theoretical Petritz mobility (Petritz, 1956) are in good agreement with the experimental values, because the average grain size, measured by electron microscopy, is comparable to

the depletion zone width, which is of the order of 20-80 nm, depending on the thermal treatment.

2. Electrical properties of a Li/InSe thin film system

The InSe films evaporated on pyrex are electrochemically active giving higher initial EMF than that of the bulk InSe. Galvanic cells with the following geometry : Li/$LiClO_4$-PC/InSe were constructed. Each cell, containing three different cathodes with the same Li reference electrode, gave initial EMF values : E = 3.3 V for InSe film (a) prepared at T_s = RT (b) and E = 2.9 V for an InSe bulk cathode (c).

The insertion of Li into films was studied first by a galvanostatic electrochemical method using a three-electrode cell : lithium metal was used for both counter and reference electrodes. An apple IIe computer was used to control the current pulse and to monitor both timing and cell voltage. As a cathode for this experiment, we used an InSe film prepared at T_s = 433 K and annealed for 50 h. at 475 K. Each step was consisted of a current pulse of I_p=1μA during 435 min., which corresponds to x = 0.05 mole of Li for the estimated cathode mass. When the cell's voltage became 0.5 V lower than the last EMF value, the

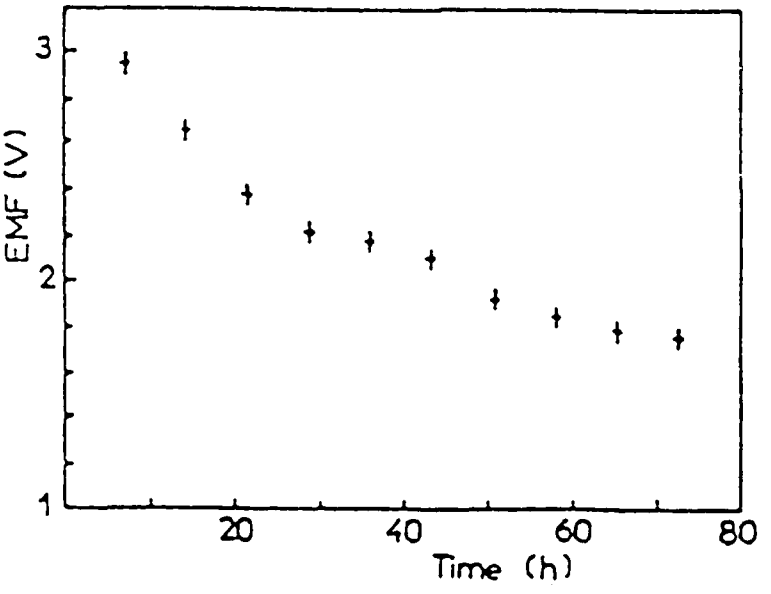

Fig.3 EMF versus time for a film InSe cathode prepared at T_s=433 K and annealed for 50 h. at 4733 K.

current pulse was switched off for 5 min. Finally the predifined charge (x = 0.05) was transferred to the cathode and the cell was left for relaxation, while the computer was recording the cell's voltage up to the point where the slope in OCV became less than 1 mV/h. The EMF of this cell for subsequent steps is presented in figure 3.

A complete voltage-composition curve has been investigated using the electrochemical potential spectroscopy (EPS) which has been developed by Thompson (Thompson,1978). This method is very useful for study of the pseudo-two-phase system as Li/InSe insertion cathode. A constant voltage is applied to the cell and this voltage is changed by a tenth of a millivolt (charge of discharge). The intensity is recorded as a function of time. When its value is low enough (i_{min}) the applied voltage is again charged by 10 mV. The full cycling of charge-discharge is automatically performed in Thompson's set-up.

Figure 4 shows the discharge curve of the InSe thin film cell. We used the InSe film prepared at T_s = 433 K and annealed for 50 h. at 475 K. The open circuit voltage versus lithium curve shows that a large flat plateau appears at 1.8 V

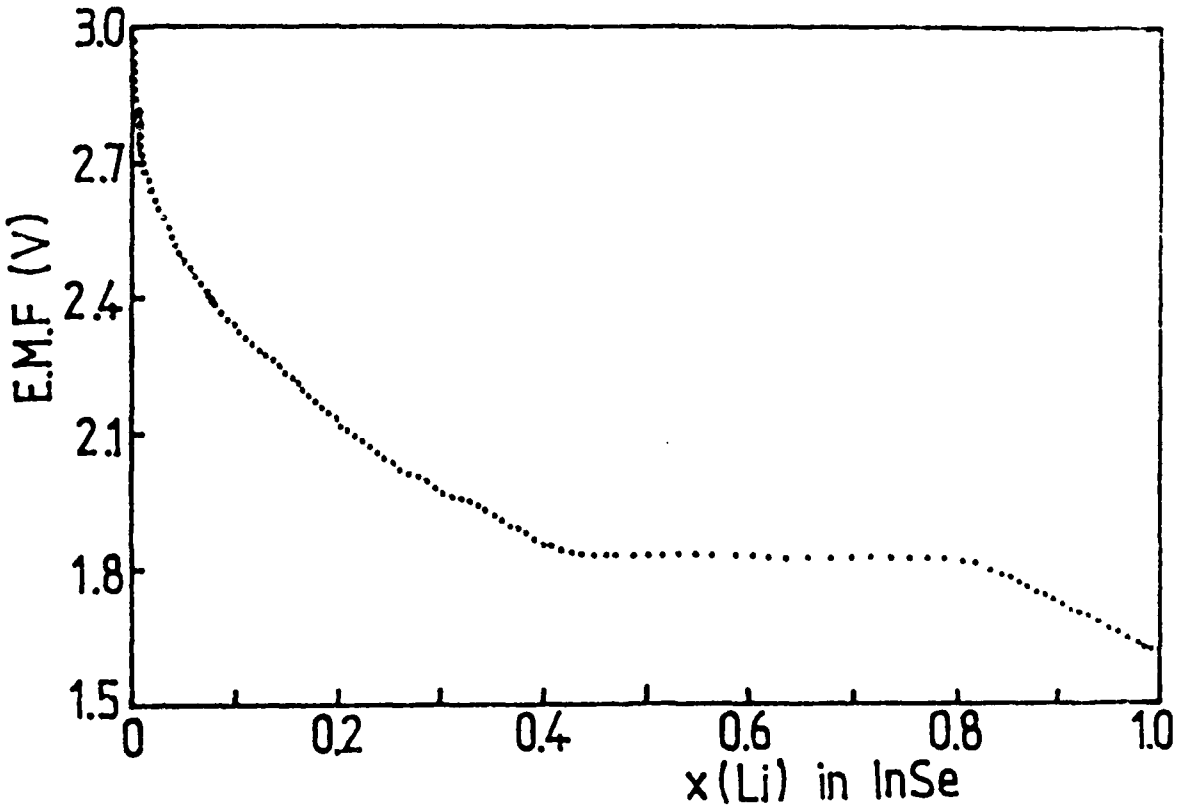

Fig.4 EMF versus x(Li) of InSe film cathode prepared at T_S=433 K and annealed during 50 hours at 475 K.

when the discharge depth reaches x = 0.4. The cathodes appeared unchanged after electrochemical cycling and no cracking or exfoliation was observed. Although no long term cycling studies were performed, the thin film InSe material was charged and discharged several times with no apparent lack of capacity.

In order to investigate the cause of the cell's polarization, the diffusivity of lithium within InSe was determined as a function of lithium composition. Using the constant current pulse method (Basu and Norrell, 1979), a plot of overvoltage versus $1/\sqrt{t}$ allows a calculation of the chemical diffusion of Li. At the end of each step we applied a current pulse of 1μA lasting 10 s. and we recorded the relaxation voltage of the cell. Figure 5 represents the Li diffusivity in InSe film annealed at 433 K for 50 h. as a function of OCV. The highest D is 4 orders lower than the corresponding value of bulk InSe.

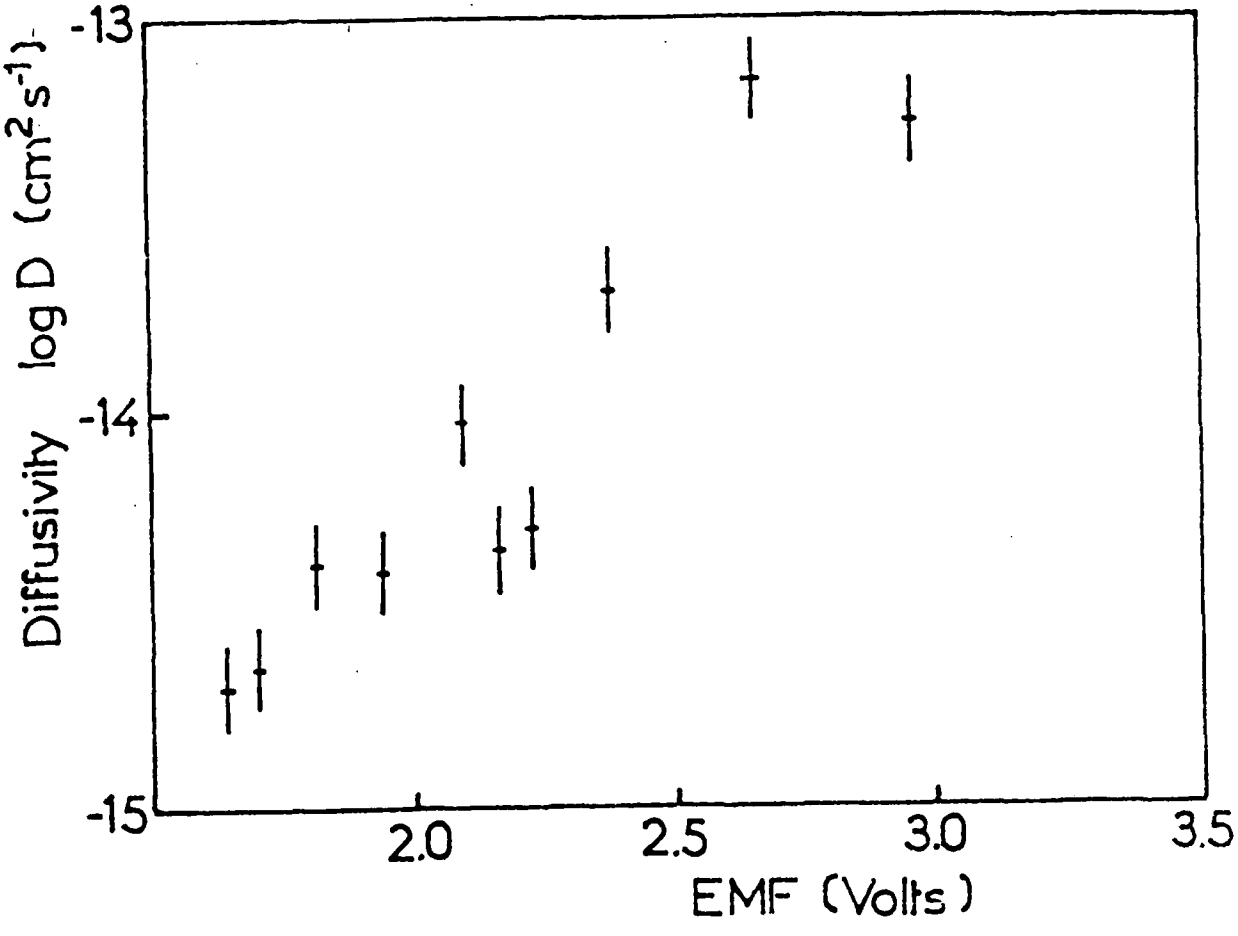

Fig. 5 Chemical diffusion coefficient versus cell's EMF using an InSe thin film as cathode.

For comparison of annealing treatment between films prepared at T_s = RT we used the linear sweep voltametry (LSV) technique (Dahn and Hearing, 1981). We observe that in non-annealed film the peak at 1.2 V is very strong compared to that of the annealed film. The apparent non-reversibility of the current peak is partly due to slow kinetics in this lower voltage range. Figure 6 shows the LSV of non-annealed film (a) and of an annealed film at T_a = 475 K during 64 h. (b).

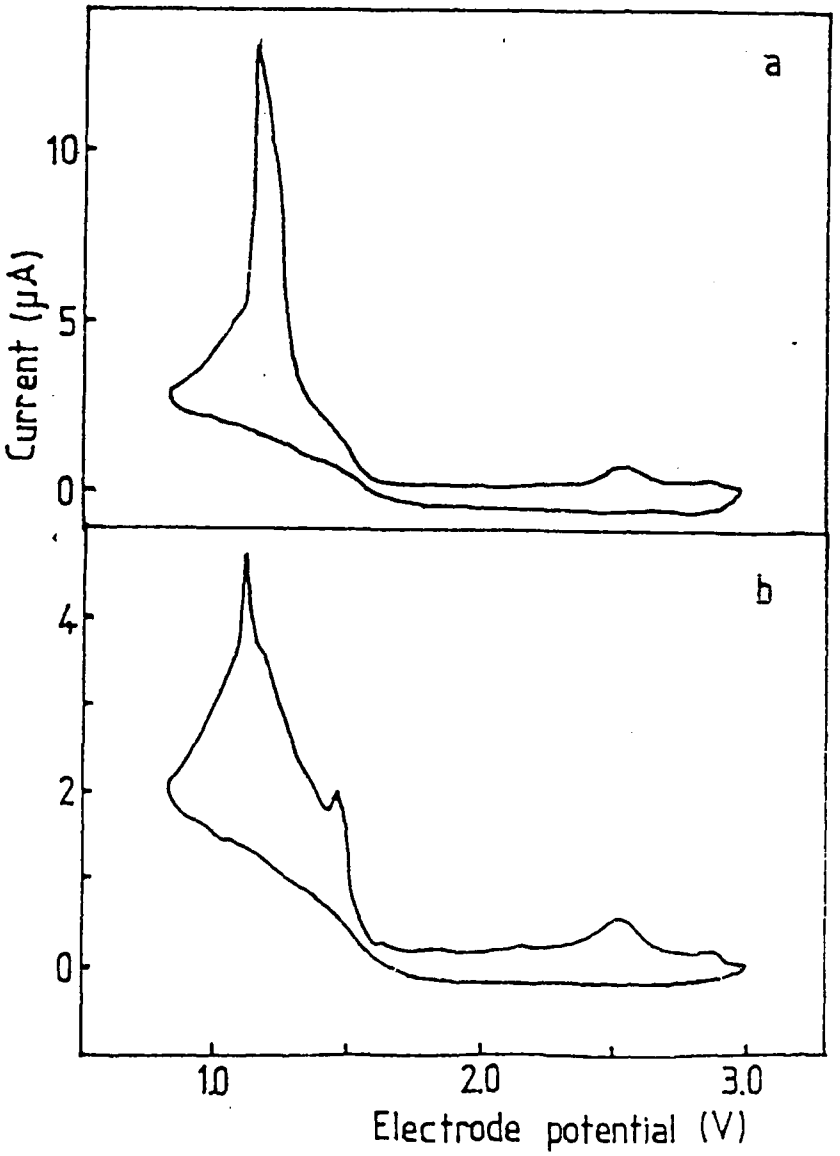

Fig. 6 Linear sweep voltagrams at 7μV/s rate of InSe films prepared at T_S=RT (a) non-annealed, (b) annealed at 475 K during 64 hours.

C. HYBRID SOLID STATE BATTERIES

1. Fast ion conducting glass

Different solid state batteries having a thickness of more than 0.5 mm and including lithium metal as alkali-ion reservoir, borate-lithium glass as solid electrolyte and lamellar compounds as insertion cathodes i.e. TiS_2 , In_2Se_3, $NiPS_3$, have been constructed and measured with the above configuration where the used separator, the solid ionic conductor which is a good electronic insulator, consists in vitreous compound of the composition B_2O_3-xLi_2O-yLiCl. The glass modifier (Li_2O) and doping component (LiCl) composition has been taken respectively x = 0.57 and 0.18 < y < 0.26 in order to obtain the higher ionic conductivity which is measured to be $\sigma = 10^{-2}\ \Omega^{-1}\ cm^{-1}$ at 300°C and of order of $10^{-4}\ \Omega^{-1}\ cm^{-1}$ at room temperature (Levasseur et al., 1980). The temperature dependence of the ionic conductivity of such solid electrolyte for definite composition is shown in figure 7. The glass having a composition of B_2O_3-0.57Li_2O-0.18LiCl which has been chosen as electrolyte is used as pressed pellet.

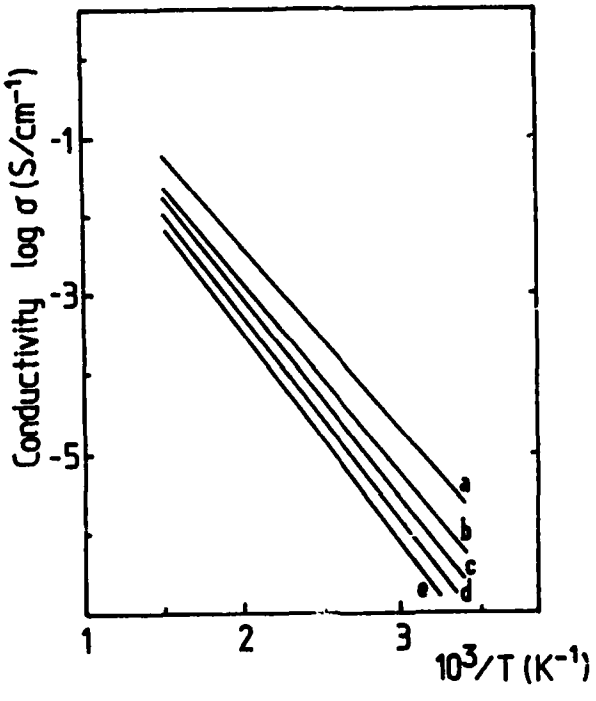

Fig. 7 Temperature dependence of the fast ionic conductor B_2O_3-xLi_2O-yLiCl of definite composition x=0.57, y=0.85 (a); x=0.85, y=0.28 (b); x=0.57, y=0.57 (c); x=0.42, y=0.28 (d) and x=0.57, y=0.21 (e).

The ionic conductivity of pressed pellets of the vitreous powder electrolyte has been studied as a function of temperature grain size and tightening pressure. The best results have been obtained with a large grain size up to 70 μm powder pressed under 12 x 10^3 kg/cm^2 (Makyta et al., 1984). Figure 8 gives the variation of log σ for a bulky glass and pressed pellet versus temperature of two grain sizes.

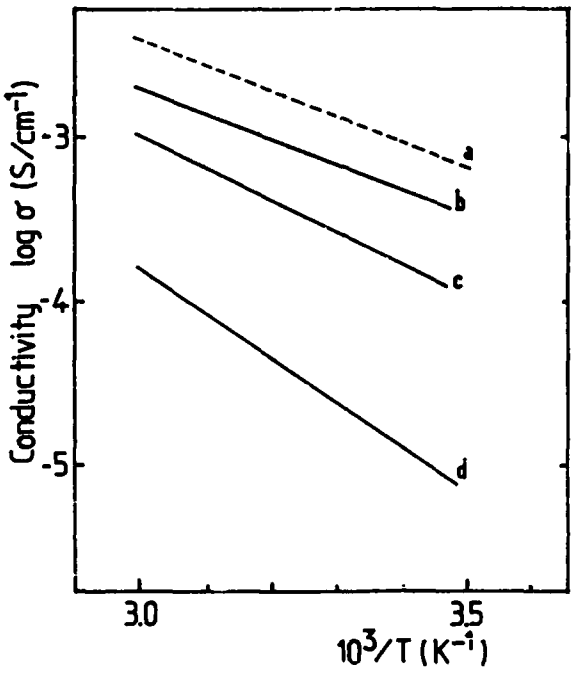

Fig. 8 Temperature dependence of the ionic conductivity of B_2O_3-0.57Li_2O-0.23LiI bulk material (a) and powdered pressed pellets with grain size up to 100μm (b) up to 45μm (c) and up to 10μm (d).

2. Cell construction

A new special cell seup has been designed. Figure 9 shows the new desing in which the solid state batterie takes place between anvils in stainless steel which are kept under in pressure using a strong spring. The external knowing is a cylinder of nylon and electrical contact are realized by direct connection on stainless steel onvils. A brass piston which is screwed into the housing allows an easy adjustement of the strength of spring.

The cell construction is shown in the figure 10. The cathode-electrolyte assembly is formed by pressing sequentially the two components in a 0.5 cm diameter steel die at room temperature. The final pressure is 10^4 kg/cm^2 and a pure lithium metal disc is then placed

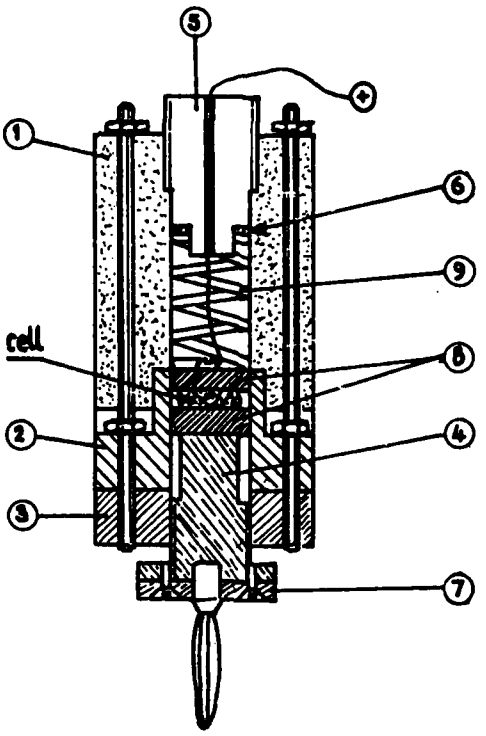

Fig. 9 Solid state batterie set-up.

on the electrode-electrolyte *composite being careful* to touch only to the electrolyte surface with the aid of an insulating mica sheet in the argon atmosphere chamber.

In this report, we present the experimental on two kinds of cells using TiS_2 and $NiPS_3$ cathodes.

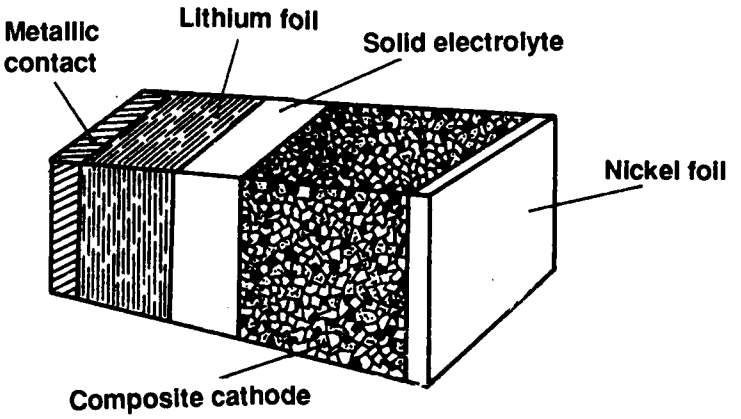

Fig. 10 Solid state cell configuration using a composite electrode with $NiPS_3$, 15% carbon and 15% fast ionic conductor.

3. Results and discussion

A series of cells of different composition have been tested. Their structures and properties are shown in table 2.

Cell no.	Structure	EMF (V)	I(μA)	IR drop (V)
1	Li/paper ($LiClO_4$-Pc) / $NiPS_3$ + 15% carbon	3.00	10	0.10
1-A	Li/B_2O_3-0.57Li_2O-0.26LiCl / $NiPS_3$	2.84	10^{-4}	0.20
1-B	Li/B_2O_3-0.57Li_2O-0.23LiI / $NiPS_3$(75%) + 15% C + 10% electrolyte	2.55	10^{-3}	0.10
2	Li / B_2O_3-0.57Li_2O-0.18LiCl/$TiS_2$85% + 15% electrolyte	2.88	10^{-2}	0.31
3	Li / B_2O_3-0.57Li_2O-0.18LiCl/$TiS_2$85% + 15% electrolyte	2.81	10	0.013
4	Li / B_2O_3-0.57Li_2O-0.18LiCl/$TiS_2$85% + 15% electrolyte	3.04	1	0.15
5	Li / B_2O_3-0.57Li_2O-0.23LiI/$TiS_2$85% + 15% electrolyte	2.90	potentiostatic measurements	

Table 2. Characteristics of the studied solid state batteries.

The results of the cell ≠ 1 are listed in table 2 and it was shown that the cathode has a good chemical diffusion coefficient. It indicates that the cathode is a good ionic conductor as well as there is a more ionic conduction on interface EL/C. Where as in cell ≠ 1-A and ≠ 1-B we have taken glass electrolyte and there were able to pass the current of nA order. We didn't get a big significant charge except the increase of the current of one order more in cell ≠ 1-B in comparison to cell ≠1-A.

current (μA)	N° of cycles (*)	D/K_t^2 ($cm^2 s^{-1}$)	D/K_t ($cm^2 s^{-1}$)	D ($cm^2 s^{-1}$)	K_t
10	After 40 cycles	2.82×10^{-8}	4.20×10^{-8}	6.26×10^{-8}	1.49
20	After 80 cycles	9.80×10^{-9}	7.73×10^{-8}	3.07×10^{-8}	1.77
20	After 130 cycles	1.15×10^{-9}	2.30×10^{-9}	4.60×10^{-9}	2.00

Table 2 : Chemical diffusion coefficients and thermodynamic (Darken) factors in cell ≠ 1.
(*) one cycle consists of a charge (1h), a discharge (1 h) and two relaxation (1 h each) all in 4 hours.

Table 3 shows the kinetic measurements of the cells ≠ 1-B and ≠ 2 respectively. From these data, it is evident that TiS_2 is a good cathode material where ionic diffusion in the cathode is much better than $NiPS_3$ and it has been verified by experiment for higher number of cycling.

cell's cathode	current I(μA)	N° of cycles	D/K_t^2 ($cm^2 s^{-1}$)	D/K_t ($cm^2 s^{-1}$)	D ($cm^2 s^{-1}$)	K_t
1-B	10^{-3}	30	3.05×10^{-8}	2.07×10^{-7}	1.32×10^{-7}	6.28
2	10^{-2}	10	7.9×10^{-7}	9.1×10^{-7}	1.04×10^{-6}	1.15

Table 3 : Chemical diffusion coefficients and thermodynamic factors in cell ≠ 1-B and ≠ 2.

The major disadvantage of those cells which we have described above is the low current draims (~ nA) as well as low energy densities. Recently in own laboratory we have succeeded to pass high currents (~μA). Through the cell configuration of type Li/B_2O_3-0.57Li_2O-0.18LiCl/TiS_2 composition (cells ≠ 3 and ≠ 4). There we have applied a new technique (Julien and Samaras, 1987) for the preparation of such kind of cell. After preparing the cell we inject one drop of $LiClO_4$-PC in anode/electrolyte interface inside the

glove box of argon atmosphere. After that the cell was dried for few hours by using rotary vacuum pump. On table 4 we are giving the kinetic results and corresponding specific energies of the cell ≠ 2 and ≠ 3 (neglecting an possible losses).

cells	current (μA)	N° of cycles	D/K_t^2 (cm^2s^{-1})	D/K_t (cm^2s^{-1})	D (cm^2s^{-1})	K_t	specific energy (Wh/kg)
3	10	After 10 cy.	1.86×10^{-6}	2.4×10^{-6}	3.16×10^{-6}	1.32	501
4	1	After 10 cy.	3.34×10^{-7}	9.08×10^{-7}	2.47×10^{-7}	2.72	505

Table 4 : Kinetic and specific energies data of cells ≠ 3 and ≠ 4.

The discharge curves of cell ≠ 3 and ≠ 4 are given in figures 11 and 12.

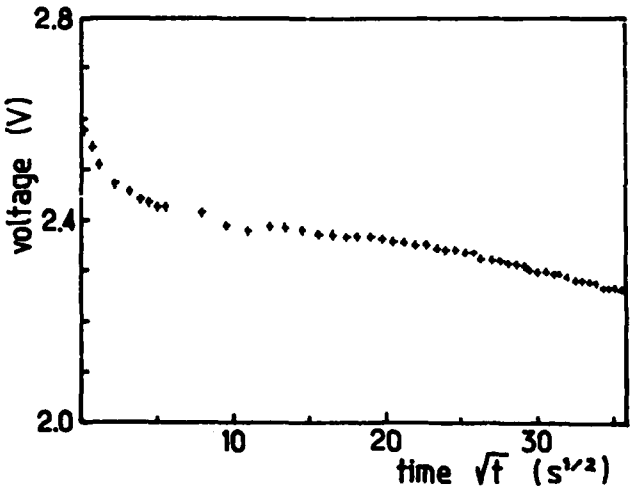

Fig.11 Discharge curve versus time of the cell n.3.

The discharge curve of the cell ≠ 3 is obtained using the configuration Li/B_2O_3-0.57Li_2O-0.18LiCl/0.85TiS_2 + 0.15 electrolyte. This cell which has a mass of 18 mg shows an overvoltage of 13 mV with a current density of 50 μA/cm^2. After a discharge during 21 hours the voltage remains higher than 2.2 V.

The kinetic parameters have been estimated using the long pulse current method

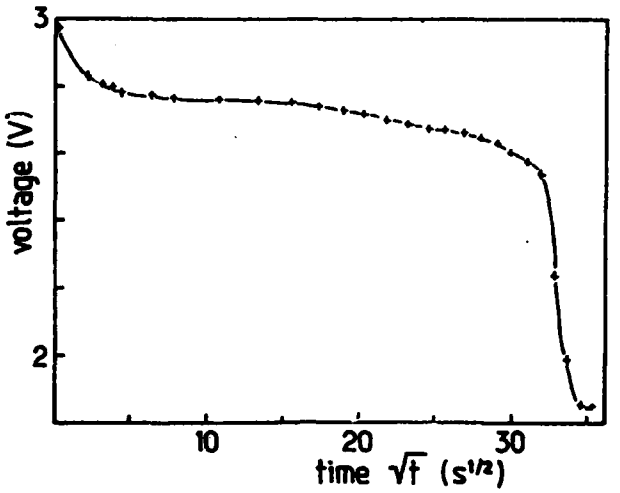

Fig. 12 Discharge curve vesus time of the cell n.4.

Honders et al., 1983). The typical transient voltage ΔE which appears after a long pulse applied to the cell shows two linear domain as function of the time. The time dependence of this transient voltage for the cell n° 4 is shown in figure 13.

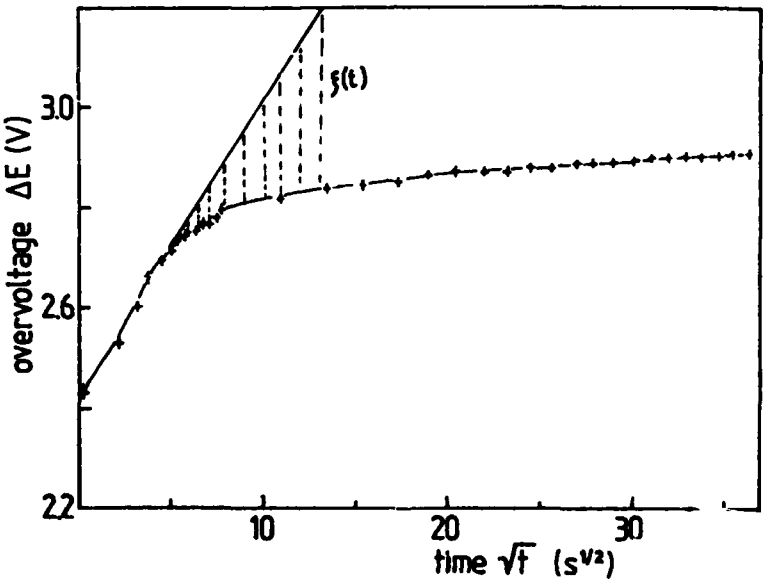

Fig. 13 Transient voltage versus $t^{1/2}$ in solid state battery Li/B_2O_3-Li_2O-LiCl/TiS_2

The time dependence of the differential voltage ζ(t) which is the deviation between the linear part of the curve and the transient voltage is represented in figure 14. The slope of this curve permits to calculate the thermodynamical factor K_t of the insertion electrode,

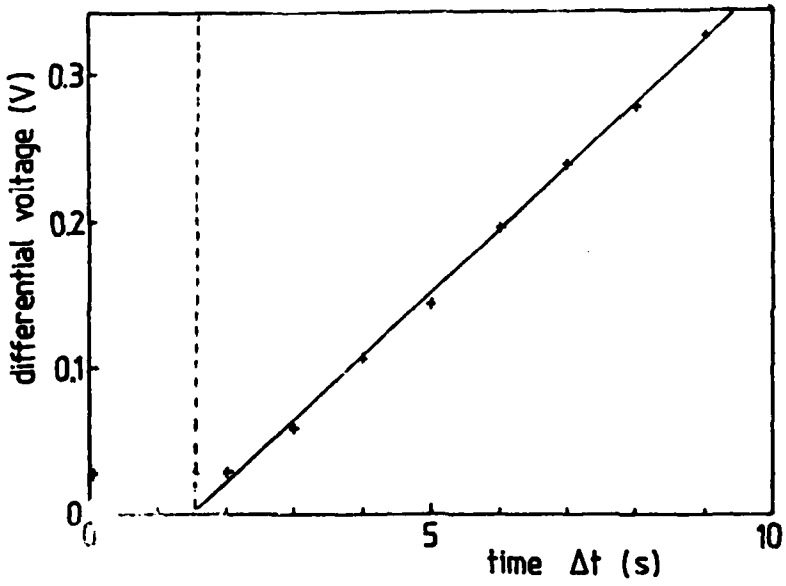

Fig. 14 Differential voltage versus time in the Li/TiS_2 cell.

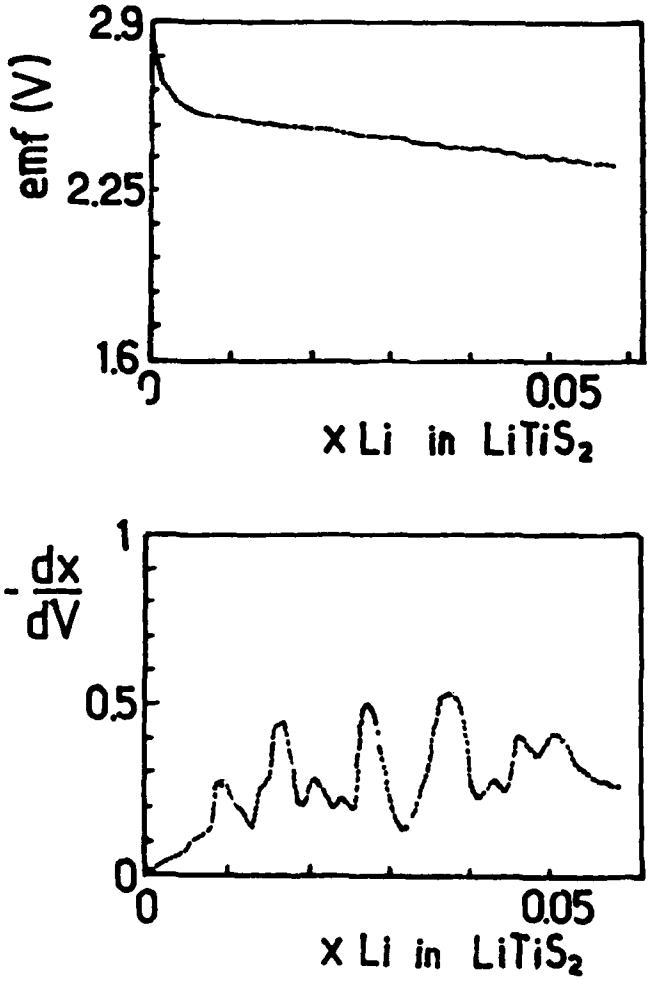

Fig. 15 Discharge-composition curve (a) and derivative voltage of a solid state battery Li/B_2O_3-Li_2O-LiCl/TiS_2 (cell n.5).

which is estimated to be less than K_t=3 in the Li/$NiPS_3$ cell cycled 10 times (figure 14).

We have studied the discharge-composition curve of a Li/TiS_2 cell using the electrochemical potentiostatic spectroscopy method. The cell's EMF and the derivative potential curve versus x(Li) in Li_xTiS_2 are shown in the figure 15. In the studied compositional range ($0 < x < 0.06$) the variation of the OCV curve is similar to thus which is ordinary observed in cells using a non-aqueous liquid electrolyte.

REFERENCES

Basu S. and Worrell W.L., 1979, in Fast Ion Transport in Solids, ed. by P. Vashishta, J.N. Mundy and G.K. Shenoy (North-Holland, Amsterdam), p. 149.

Dahn J.R. and Hearing R.R., 1981, Solid State Ionics, **2**, 19.

Guesdon J.P., Kobbi B., Julien C. and Balkanski M., 1987, Phys. Stat. Sol. (a),**102**, 327.

Julien C. and Hatzikraniotis E., 1987, Materials Letters, **5**, 134.

Julien C. and Samaras I., 1987, Int. LPS. Report **3**.

Kanehori K., Matsumoto K., Migauchi K. and Kudo T., 1983 Solid State Ionics, **9-10**, 1469.

Levasseur A., Brethous J.C., Reau J.M., Hagenmuller P. and Couzi M., 1980, Solid State Ionics, **1**, 177.

Makyta M., Levasseur A. and Hagenmuller P., 1984, Mat. Res. Bull., **19**, 1361.

Menetrier M, Levasseur A., Delmas C., Audebert J.F. and Hagenmuller P., 1984 Solid State Ionics, **14**, 257.

Petritz R.L., 1956, Phys. Rev., **104**, 1508.

Thompson A.H., 1978, Phys. Rev. Lett., **46**, 1511.

END
DATE
FILMED
7-88
DTIC